# Transient Nonisothermal Fully Coupled Wellbore/Reservoir Model for Gas-Well Testing, Part 1: Modelling

**M. Bahonar,** SPE, **J. Azaiez,** and **Z. Chen,** SPE, University of Calgary

## Summary

A numerical fully implicit nonisothermal wellbore/reservoir simulator is developed. The model entails simultaneous solution of transient coupled mass-, momentum-, and energy-balance equations within the wellbore; energy-balance equations for the tubular and cement materials and the formation surrounding the wellbore; and mass-balance and flow-rate/pressure equations for the reservoir formation. A wellbore heat-loss model that is a strong feature of this study is developed and employed in the model to improve the accuracy of the simulator and to be able to estimate the casing temperature and formation-temperature distribution. The model formulation is completed with an equation of state (EOS) to estimate fluid properties and appropriate friction-factor correlations in the wellbore tubing to compute the frictional pressure drop for different flow regimes.

The developed model has several applications in the petroleum industry, particularly in the gas-well testing design and interpretation of both isothermal and nonisothermal gas reservoirs.

This nonisothermal simulator is validated through comparisons to both analytical models and an equivalent numerical isothermal coupled wellbore/reservoir simulator that is also developed in this paper. Applications of this simulator to analyzing gas-well testing problems, in addition to several important observations, are extensively studied in Part 2 of this research work (Bahonar et al. 2010).

Currently, it has been well accepted that the applicability and significance of a reservoir simulator depend on the behaviour of the wellbore and interaction between the wellbore and reservoir. A robust, accurate coupled wellbore and reservoir simulator is an invaluable tool for the petroleum engineer to help the petroleum industry understand production behaviour, make a meaningful prediction, and make correct decisions in all field-development and production stages.

## Introduction

From the late 1920s, important petroleum-engineering aspects have been developed, including measurements of bottomhole pressure (BHP) and bottomhole temperature (BHT), petroleum laboratory experiments, petrophysical concepts, introduction of fluid saturations, development of material-balance techniques, and numerous other reservoir-engineering concepts (Craft et al. 1991). During the 1960s, reservoir simulation became popular and expanded quickly with the aid of the invention of high-speed digital computers and development of powerful numerical techniques that allowed solving more-complicated problems. In 1962, a pioneering work in wellbore modelling was presented by Ramey (1962). Ramey's analytical model was derived on the basis of several simplifying assumptions, including neglecting the friction and kinetic energy, and estimates the fluid temperature along the wellbore as a function of time and depth. To apply this model for more-complex situations, several investigators (Satter 1965; Holst and Flock 1966; Wilhite 1967; Farouq Ali 1981; Fontanilla and Aziz 1982; Yao 1985; Wu and Pruess 1990; Sagar et al. 1991; Alves et al. 1992; Hasan and Kabir 1994) proposed improvements to Ramey's model. Research in reservoir simulation also progressed rapidly but was fairly separated from wellbore modelling until it was realized that these two systems may have significant impacts on each other in some applications and hence must be considered together.

One of the earliest numerical coupled wellbore/reservoir simulators was developed by Miller (1980) to study the reservoir and wellbore fluid-flow interactions. Effects of temperature changes during well testing of geothermal wells were also investigated. Subsequently, several other coupled wellbore/reservoir simulators have been developed that can be classified into two primary groups.

The first group encompasses general-purpose numerical reservoir simulators. These simulators are capable of solving nonisothermal (Stone et al. 1989; Stone et al. 2002; Pourafshary et al. 2009; Shirdel and Sepehrnoori 2009; Livescu et al. 2010; Semenova et al. 2010) or isothermal (Stone et al. 2002; Semenova et al. 2010) multiphase-flow problems and were primarily designed to run full-field simulations with several wells. Among these simulators, ones presented by Stone et al. (2002), Pourafshary et al. (2009), Shirdel and Sepehrnoori (2009), and Semenova et al. (2010) are general compositional models and others developed by Stone et al. (1989), Stone et al. (2002), Livescu et al. (2010), and Semenova et al. (2010) are black-oil models; the simulator of Semenova et al. (2010) contains both compositional and black-oil models. The newest multisegment simulator of Stone et al. (2002), which is an extension of an earlier model, includes nonisothermal and isothermal black-oil models and an isothermal compositional model. Both models by Livescu et al. (2010) and Semenova et al. (2010) stemmed from Stanford's general-purpose research simulator, having the capability of modelling complex well trajectories (deviated, multilateral, and horizontal wells). The main difference is that the Semenova et al. (2010) model was developed for both compositional and black-oil models, while the Livescu et al. (2010) model was based only on the black-oil model. Similarly, Pourafshary et al. (2009) and Shirdel and Sepehrnoori (2009) implemented their models into the general-purpose adaptive simulator from The University of Texas at Austin. The core difference between the Pourafshary et al. (2009) and the Shirdel and Sepehrnoori (2009) models is that the latter is for horizontal wells, whereas the former was developed for vertical wells.

The second group to which our model also belongs includes coupled wellbore/reservoir models that are to a large extent less general than the first group. However, these models can be used more efficiently and sometimes more accurately than the models in the first group to investigate well-testing problems. The reason is that they were particularly intended for this purpose and contain a standing-alone well (a single well coupled with a reservoir model). Examples of such models include those by Kabir et al. (1996), Fan et al. (2000), Hasan et al. (2005), and Izgec et al. (2007).

The transient coupled gas-wellbore/reservoir simulator presented by Kabir et al. (1996) was developed to run in two modes. The first one is a forward modelling to estimate the BHP, wellhead pressure (WHP), and wellhead temperature (WHT) for a given reservoir and given well completion data. In contrast to the first mode, the second one is a reverse modelling to translate recorded WHP

Original manuscript received for review 20 September 2010. Revised manuscript received 7 March 2011. Paper (SPE 149617) peer approved 3 May 2011.

and WHT to BHP. These two modes are valuable tools for transient well-test design and interpretation. In addition, they are excellent tools for obtaining invaluable information for a hostile downhole environment of high- pressure/high-temperature (HP/HT) gas reservoirs in which running well testing is difficult, expensive, and time consuming. This condition may become more severe with the presence of corrosive and sour gases (e.g., carbon dioxide and hydrogen sulfide) that add the possibility of failure of equipment at extreme conditions. To give a sense about HP/HT gas reservoirs, the BHT and BHP greater than 400°F and 11,000 psia, respectively, with the presence of corrosive gases, have been reported in the literature (Kabir et al. 1996). As a result of technological, operational, and economic challenges in the well testing of these HTHP gas reservoirs reported by Kabir et al. (1996), the cost of recording BHP in such hostile environments can easily exceed several million dollars. Therefore, gas-well testing is sometimes carried out on the basis of WHP measurements, and coupled wellbore/reservoir simulators are invaluable tools to assist in this task.

Fan et al. (2000) developed a semianalytical gas-wellbore/reservoir model to describe the wellbore's nonisothermal effects on the pressure-buildup test. The major assumption in this model is that the well has been producing for a long period of time and the steady-state condition has been reached inside the wellbore before a buildup test. This assumption limits their model solely for the buildup test; and drawdown test and multirate tests cannot be modelled. Other simplifying assumptions, particularly in the energy-balance equation, were taken into account, and the final form of equations was solved with sequential and iterative schemes. It was shown that if thermal effects are not considered properly in gas-buildup tests, the interpretation of data using well-testing software may become misleading. For instance, the dual-porosity behaviour may be seen for the well testing of nonisothermal conventional homogeneous gas reservoirs. Another interesting case that results from neglecting nonisothermal effects in the interpretation of data with well-testing software, but for a conventional heterogeneous gas reservoir, will be presented in Part 2 of this study (Bahonar et al. 2010). The reason that using the well-testing software for well-testing design, analysis, and interpretation of nonisothermal gas reservoirs may lead to improper test design and/or wrong interpretation resides in the assumptions used in the software. The well-testing software solves only a single equation (i.e., the diffusivity equation) for an isothermal reservoir with analytical methods. The full solution of the diffusivity equation contains a series of infinite Bessel functions. However, only some limiting approximate forms (e.g., an infinite cylindrical reservoir with a line-source well or the pseudosteady-state solution) of the full solution are used. This equation does not obviously consider wellbore dynamics, interaction of the wellbore and reservoir, or nonisothermal effects of the wellbore and its surrounding media, among other factors. Additionally, the equation is not able to properly model the well-testing operation of HP/HT gas reservoirs in which the well is shut-in at the wellhead because it simply solves the diffusivity equation only and disregards the wellbore and its surrounding media. Therefore, the well-testing software is blind with respect to the aforementioned factors.

Hasan et al. (2005) developed a simple analytic model for the computation of transient temperature along the wellbore for both shut-in and flowing wells. To achieve this, they imposed some assumptions, including zero-mass flux during a buildup and a constant-mass flux during drawdown tests on their previous coupled wellbore/reservoir simulator (Kabir et al. 1996). They found a good agreement between the newer model (Hasan et al. 2005) and the previous one (Kabir et al. 1996). Through some parametric studies, they also demonstrated that the reservoir-flow capacity (permeability × reservoir formation thickness) had the most profound influence on the quality and suitability of WHP/WHT measurements to convert them to BHP and thus conduct the transient well-test analysis. The conclusion was that the higher the reservoir-flow capacity, the less worthy to translate the WHP/WHT to BHP. Izgec et al. (2007) further improved the previous analytic heat-transfer formulations (Kabir et al. 1996; Hasan et al. 2005) by removing a constant parameter [called a relaxation-parameter, which is the inverse of a parameter formerly defined by Ramey (1962)] assumption. They also enhanced the estimation of formation temperature by performing a simple steady-state energy balance on a small-volume element in the instant vicinity of the wellbore. However, this volume-element thickness was treated as a history-matching parameter in their model.

The model developed in this study has a number of characteristics that distinguish it from previous models. Unlike the models developed by Livescu et al. (2010) and Semenova et al. (2010) that used a constant overall heat-transfer coefficient for heat-loss modelling, which is not the case in real wells, we develop and apply a strong heat-loss model. Indeed, the importance of accurate modelling of the overall heat-transfer coefficient has been emphasized by several investigators repeatedly [e.g., see work in geothermal wells by Hasan and Kabir (2009)]. Furthermore, the models by Pourafshary et al. (2009) and Shirdel and Sepehrnoori (2009), and all models in the second group of coupled wellbore/reservoir simulators, adopted approximate analytical models for heat-loss treatment. The present study, on the other hand, is based on a robust fully implicit formulation for the modelling of heat loss from the wellbore to the surrounding medium that is fully coupled with the energy-balance equation inside the wellbore. This improvement removes several limitations and weaknesses associated with previous approximate analytical models (Bahonar et al. 2011). The equation allows estimation of the casing temperature and formation-temperature distribution around the wellbore, removes the need for the application of the superposition principle in the analytical models, and employs a nonlinear transient depth- and temperature-dependent overall heat-transfer coefficient for additional accuracy. In contrast to the models of Pourafshary et al. (2009) and Shirdel and Sepehrnoori (2009) that assumed the steady-state condition in the wellbore, which is not accurate for transient tests, our model is fully transient. Note that some important phenomena in transient tests will happen during initial times of shut-in or flowing and thus their accurate modelling becomes essential. Moreover, unlike all models of the second group that applied analytical reservoir models and used correlations for estimating fluid properties, we used a more general formulation and applied the Peng-Robinson (Peng and Robinson 1976) EOS (PR EOS) to estimate fluid properties. This way, the EOS can be tuned for any gas mixture with laboratory experiments; thus, removing the limitations caused by correlations. In contrast to the model of Fan et al. (2000) that can be used only for a gas-buildup test, our model can be used for any production or injection schedule (multirate) combined with shut-in periods at any time interval. During shut-in periods, our model can imitate the afterflow phenomenon accurately. Because of its fully implicit, fully coupled nature, our model can be run for shallow to extremely deep reservoirs (in this case, the EOS must be tuned for HP/HT conditions), small to large timestep sizes, and small to large wellbore-segment length. Furthermore, by performing some simple modifications as performed in this work, this nonisothermal simulator can be converted to its isothermal counterpart.

This paper proceeds as follows. We first describe the formulation of fluid flow and heat transfer in the coupled reservoir, wellbore, tubular and cement materials, and formation. The discretization of equations and the solution methodology are explained next. Subsequently, we validate the results of the simulator against analytical models employed in well-testing software. We also compare a result of the nonisothermal model with a result of its isothermal counterpart. Last, conclusions will be presented.

Several numerical experiments for both nonisothermal and isothermal models developed in this paper have been carried out. Comparisons of these results and some unusual thermal effects on the transient well tests are described in Part 2 of this research study (Bahonar et al. 2010).

## Model Development

The overall system is divided into three major parts: reservoir, wellbore, and tubular and cement material and formation. **Fig. 1**

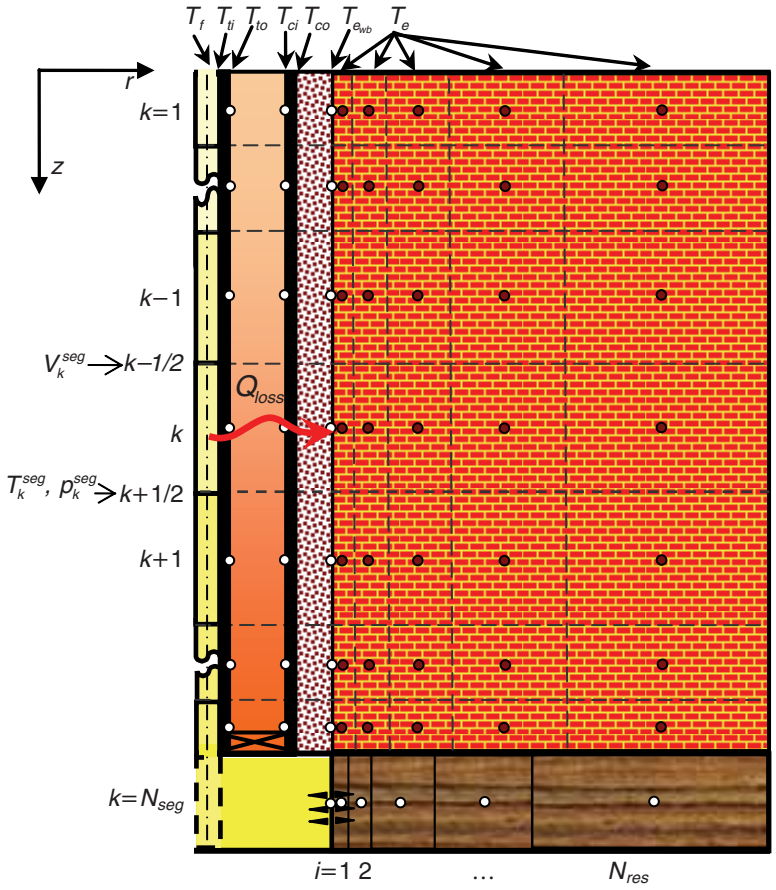


**Fig. 1—Schematic representation of the discretized reservoir, wellbore, and formation (earth).**

sketches the entire system. To avoid confusion, from now on we call the reservoir formation the "reservoir" and the earth media surrounding the wellbore the "formation."

## Reservoir

**Mass-Balance Equation and Flow-Rate/Pressure Relationship.** 1D radial gas flow is considered for the reservoir. The mass-conservation equation for the gas component is

$$\frac{1}{\alpha_0}\frac{\partial}{\partial t}\left(\phi\rho\left(1-s_{wc}\right)\right)+\frac{1}{r}\frac{\partial}{\partial r}\left(r\rho u_r\right)+m'=0, \quad \ldots\ldots\ldots\ldots (1)$$

where the terms from the left to right represent the gas-mass accumulation, gas-convective flux, and source/sink term, respectively. The source/sink term $m'$ couples the reservoir mass-balance equation to the corresponding mass-balance equation inside the wellbore.

With the definition of the gas-formation-volume factor given in Eq. 2, the mass-balance equation can be written in a more appropriate form as Eq. 3:

$$B_g=\frac{\rho_{sc}}{\alpha_0\rho}=\frac{p_{sc}}{\alpha_0 T_{sc}}\frac{z_g T}{p} \quad \ldots\ldots\ldots\ldots (2)$$

$$\frac{V_b}{\alpha_0}\frac{\partial}{\partial t}\left(\frac{\phi\left(1-s_{wc}\right)}{B_g}\right)+\frac{V_b}{r}\frac{\partial}{\partial r}\left(\frac{ru_r}{B_g}\right)+\frac{m}{\rho_{sc}}=0 \quad \ldots\ldots\ldots\ldots (3)$$

In Eq. 3, $m$ is the mass-flow rate across the perforation and is given by

$$m=\rho_{sc}q_{sc}, \quad \ldots\ldots\ldots\ldots (4)$$

where the mass-flow rate $m$ and the volumetric-flow rate $q$ are positive for production and negative for injection. The volumetric-flow rate is the product of the difference between the reservoir and wellbore pressure and the wellbore transmissibility.

The rock porosity change is linearly related to the pressure variation by rock-compressibility factor $c_R$. The effect of water compressibility on the reservoir pore-volume changes during the reservoir-pressure variation is considered by merging the saturation-weighted water compressibility, $s_{wc}\times c_w$ into the rock compressibility as

$$\phi=\phi_{ref}\left[1+c'_R\left(p-p_{ref}\right)\right], \quad \ldots\ldots\ldots\ldots (5)$$

where $c'_R=c_R+s_{wc}c_w$ is the combined rock and saturation-weighted water compressibility. Darcy's law is used for the flow-rate/pressure relationship as

$$u_r=-\beta_0\frac{k_r}{\mu_g}\left(\frac{\partial p}{\partial r}\right), \quad \ldots\ldots\ldots\ldots (6)$$

where $\beta_0$ is an appropriate conversion factor for desired units.

## Wellbore

**Mass-Balance Equation.** The general 1D axial mass-balance equation for the wellbore is

$$A\frac{\partial}{\partial t}(\rho)+\frac{\partial}{\partial z}(\rho VA)-\frac{m}{\Delta L}=0, \quad \ldots\ldots\ldots\ldots (7)$$

where the first term is the mass accumulation, the second term is the mass-convective flux, and the last term is the source/sink term.

**Momentum-Balance Equation.** The momentum-balance equation can be written as (Farouq Ali 1981; Kabir et al. 1996; Hasan and Kabir 2002; Hasan et al. 2005; Livescu et al. 2010; Semenova et al. 2010)

$$\beta_1 \frac{\partial p}{\partial z} = -\rho g \cos(\theta) - \frac{f\rho V|V|}{2d} - \frac{\partial}{\partial t}(\rho V) - \frac{\partial}{\partial z}(\rho V^2) \quad \text{..... (8)}$$

Expanding the last two terms in Eq. 8 and combining with the mass-balance equation for the wellbore leads to

$$\beta_1 \frac{\partial p}{\partial z} = -\rho g \cos(\theta) - \frac{f\rho V|V|}{2d} - \rho V \frac{\partial V}{\partial z} - \rho \frac{\partial V}{\partial t} - \frac{m \times V}{\Delta L \times A}, \quad \text{... (9)}$$

where different components of the pressure drop inside the wellbore from the left to right are hydrostatic, frictional, acceleration, unsteady-state pressure loss, and pressure drop across the perforation, respectively. Correlations for estimating the value of the friction factor $f$ are given in Appendix A for both smooth and rough pipes and both laminar- and turbulent-flow regimes. Note that the absolute-velocity term in the frictional loss is used to properly handle the situation in which the direction of flow changes.

**Energy-Balance Equation.** The energy-balance equation can be expressed as (Farouq Ali 1981; Kabir et al. 1996; Hasan and Kabir 2002; Hasan et al. 2005; Livescu et al. 2010; Semenova et al. 2010)

$$(1+C_T)\frac{\partial}{\partial t}\left[\rho\left(u+\frac{V^2}{2g_cJ_c}\right)\right]+\frac{1}{A}\frac{\partial}{\partial z}\left[\rho VA\left(h+\frac{V^2}{2g_cJ_c}\right)\right] \quad \text{.... (10)}$$
$$-\frac{g}{g_cJ_c}\rho V\cos(\theta)+\frac{Q_{loss}}{A}-\frac{m_h}{V_b^{seg}}+\frac{1}{\mathrm{A}}\frac{\partial}{\partial z}\left(k_f A\frac{\partial T^{seg}}{\partial z}\right)=0$$

where the terms from the left to the right are energy accumulation, convective-energy flux, work performed by pressure forces, the rate of work performed on the fluid by gravitational forces, heat loss to the wellbore surroundings, energy source/sink, and conductive heat transfer in the axial direction, respectively. In Eq. 10, the energy source/sink term is simply multiplication of the mass-source/sink term in the mass-balance equation (Eq. 7) by the fluid enthalpy (i.e., $m_h = m \times h$). Because no thermal accumulation is considered for the tubular and cement materials surrounding the wellbore, it is assumed that the energy accumulation in these components is a fraction of fluid-energy accumulation inside the wellbore at any time. This assumption is incorporated into the energy-balance equation by defining a thermal-storage parameter, $C_T$. The concept of $C_T$ has been introduced by Hasan and Kabir (2002). It has also been shown that this parameter is 3.0 for their drawdown and 2.0 for the buildup tests (Hasan et al. 2005). The heat-loss term is derived by the difference between fluid temperature inside the wellbore and wellbore temperature, and the value of the overall heat-transfer coefficient, as

$$Q_{loss} = 2\pi r_{to} U_{to}\left(T^{seg} - T_{e_{wb}}\right) \quad \text{..... (11)}$$

### Cement and Tubular Materials and Formation

Equations for calculating the temperatures of tubing outside and casing inside, respectively, are given in the following paragraph, and more details can be found in the paper by Bahonar et al. (2011):

$$T_{to} = T^{seg} - \left[\ln(r_{to}/r_{ti})/k_t\right] r_{to} U_{to}\left(T^{seg} - T_{e_{wb}}\right) \quad \text{..... (12)}$$

$$T_{ci} = T_{e_{wb}} + \left[\ln(r_{wb}/r_{co})/k_{cem} + \ln(r_{co}/r_{ci})/k_c\right] r_{to} U_{to}\left(T^{seg} - T_{e_{wb}}\right) \quad \text{..... (13)}$$

Expressions for the wellbore and formation temperatures can be obtained in analogy to the fluid flow in the reservoir. The wellbore temperature ($T_{e_{wb}}$) can be calculated from the amount of heat loss, formation temperature, and formation geometric factor. The equation that contains the wellbore temperature is

$$Q_{loss} = \Psi_r\left(T_{e_{wb}} - T_e\right), \quad \text{..... (14)}$$

where the thermal geometric factor $\Psi_r$ is mainly a function of formation thermal conductivity and thermal skin, *TSkin*, caused by thermal resistance (temperature drop) across the cement/formation interface. This function can be expressed as

$$\Psi_r = \Psi_r\left(k_{er},\ TSkin\right) \quad \text{..... (15)}$$

An expression for calculating the thermal geometric factor will be presented later.

A transient-heat-conduction partial-differential equation (PDE) with a source term in the 2D-cylindrical-coordinate system is considered for the formation temperature as

$$\frac{1}{r}\frac{\partial}{\partial r}\left(k_{er} r \frac{\partial T_e}{\partial r}\right)+\frac{\partial}{\partial z}\left(k_{ez}\frac{\partial T_e}{\partial z}\right)+\frac{Q_{loss}}{A_z}=\rho_e C_{pe}\frac{\partial T_e}{\partial t} \quad \text{..... (16)}$$

Note that in Eq. 16, the formation thermal conductivity, density, and heat capacity can vary in both axial and radial directions. As we show later in Eq. 41, the geothermal temperature gradient can also be different for different layers. Therefore, a multilayer formation with different properties and geothermal temperature gradients can be modelled by this treatment.

## Auxiliary Equations

To complete the model formulation, some auxiliary equations should be implemented into the model. Some of the most important ones are explained here. The PR EOS (Peng and Robinson 1976) for gas mixtures with hydrocarbon/hydrocarbon and nonhydrocarbon/hydrocarbon binary-interaction coefficients is used. Entering the PR EOS into an enthalpy departure function (Sandler 2006), and adding this function to the enthalpy of an ideal-gas mixture that is only a function of gas temperature [data in terms of a fifth-order polynomial for 89 compounds, mostly hydrocarbons can be obtained from the paper by Passut and Danner (1972)], the value of enthalpy for the real-gas mixture can be estimated. The Joule-Thomson effect is inherently included in the model through the general treatment of the enthalpy, as previously stated. In fact, the Joule-Thomson coefficient can be simply calculated from the derivatives of the enthalpy with respect to pressure and temperature as $-(\partial h/\partial p)_T/(\partial h/\partial T)_p$. Once enthalpy and other fluid properties, in addition to their derivatives with respect to both pressure and temperature, are obtained, the internal energy can be readily calculated from the enthalpy/internal-energy relationship. This relationship indicates that the internal energy is equal to enthalpy minus the ratio of pressure to the fluid density, all in appropriate units.

An appropriate viscosity correlation recommended by Computer Modelling Group's WinProp user's guide (WinProp Phase Property Program 2009) for the gas mixture—based on the critical temperature, critical pressure, critical molar volumes, and molecular weight—is used. The PR EOS (Peng and Robinson 1976) and viscosity correlation can be easily tuned to match the laboratory-measured data for any gas mixture.

The overall heat-transfer coefficient is an extremely important parameter for accurate heat-loss calculation and must be honoured appropriately (Hasan and Kabir 2009). To estimate this coefficient, a series of heat resistances for the tubing, wellbore annulus, casing, and cementing is considered. The main heat-transfer mechanism in all these layers is conduction. However, convection and thermal radiation are also present in the wellbore annulus, which makes the overall heat-transfer coefficient a nonlinear transient tempera-

ture- and depth-dependent parameter. We followed the procedure presented by Wilhite (1967) to estimate this parameter, in which the radiative heat-transfer coefficient is calculated by the Stefan-Boltzmann law and the convective heat-transfer coefficient is correlated with the Grashof and Prandtl numbers.

## Numerical Implementation

Both the reservoir and formation are gridded in radial-cylindrical coordinates, as shown in Fig. 1. The geometric factors, gridblock volume, centre, and boundary positions for the anisotropic reservoir/formation and irregular gridblock distribution in the 2D-cylindrical-coordinate system are given in Appendix B. The reason that we provide these expressions in the 2D-cylindrical coordinates in spite of the 1D reservoir assumption is that the same grid system with minor modifications is used for the formation section that is a 2D system. The wellbore is discretized into $N_{\text{seg}}$ segments, and staggered grids are used, as depicted in Fig. 1. For Segment $k$, the temperature and pressure are assigned to the lower boundary (entrance in the case of production) and the velocity is assigned to the upper boundary (exit in the case of production). All fluid and wellbore properties are considered to be constant within each segment. A first-order upwind scheme is used for reservoir transmissibilities and the mass- and energy-balance equations in the wellbore. The upwind scheme is switched if the direction of flow changes in the reservoir or wellbore. All governing equations are discretized in a fully implicit scheme (which will be shown by the superscript $n+1$ on all variables) to speed up the convergence, but this results in a system of nonlinear equations. These equations are then written in the residual forms, as follows.

## Reservoir

**Combined Mass-Balance Equation and Flow-Rate/Pressure Relationship.** Combining Eqs. 3 and 6 and performing some manipulations lead to the final form of the mass-balance equation in the residual form:

$$R^{n+1}_{mR_i}=\left[T^{n+1}_{i-1/2}\left(p^{n+1}_{i-1}-p^{n+1}_{i}\right)+T^{n+1}_{i+1/2}\left(p^{n+1}_{i+1}-p^{n+1}_{i}\right)\right] -\frac{m^{n+1}_{sc_i}}{\rho_{sc}}-\Gamma^{n+1}_{i}\left(\frac{p^{n+1}_{i}-p^{n}_{i}}{\Delta t^{n+1}}\right)=0 \quad , \quad \text{..... (17)}$$

where $\Gamma^{n+1}_{i}$ is given by

$$\Gamma^{n+1}_{i}=\frac{V_{b_i}\left(1-s_{wc}\right)}{\alpha_0}\left[\frac{\phi_{ref}c'_R}{B^{n+1}_{g_i}}+\frac{\phi^{n}_{i}}{B^{n}_{g_i}}\left(\frac{B^{n}_{g_i}/B^{n+1}_{g_i}-1}{p^{n+1}_{i}-p^{n}_{i}}\right)\right] \quad \text{..... (18)}$$

In Eq. 18, $\left(B^{n}_{g_i}/B^{n+1}_{g_i}-1\right)/\left(p^{n+1}_{i}-p^{n}_{i}\right)$ is the averaged gas compressibility between $p_i^{n+1}$ and $p_i^n$. In fact, discretizing the time-derivative term in the material-balance equation (only in the form given in Eqs. 17 and 18) is materially conserved, as proved by Ertekin et al. (2001).

In Eq. 17, the transmissibility terms between any two adjacent gridblocks are calculated by

$$T^{\text{n+1}}_{i\pm1/2}=\left(\beta_0\frac{k_rA_r}{\mu_gB_g\Delta r}\right)^{\text{n+1}}_{i\pm1/2}=\left(\beta_0\frac{k_rA_r}{\Delta r}\right)_{i\pm1/2}\left(\frac{1}{\mu_gB_g}\right)^{\text{n+1}}_{i\pm1/2} , \\ =G_{i\pm1/2}\left(\frac{1}{\mu_gB_g}\right)^{\text{n+1}}_{i\pm1/2} \quad \text{..... (19)}$$

where $i=1, 2, \ldots, N_{res}$, except for $T^{\text{n+1}}_{1-1/2}$ and $T^{\text{n+1}}_{N_{res}+1/2}$ that will be explained later as the boundary conditions (BCs). In the transmissibility expressions, $A_r=2\pi\Delta zr$ is the area crossed by the flow and $G_{i\pm1/2}$ is the geometric factor, as given in Appendix B. Note that the reservoir permeability can vary in the radial direction; therefore, composite reservoirs can be modelled readily.

As the inner reservoir BC, the first gridblock of the reservoir is coupled with the last one of the wellbore grid across the perforation by the mass-sink/source term:

$$\frac{m^{n+1}}{\rho_{sc}}=q^{n+1}_{sc_{1-1/2}}=T^{n+1}_{1-1/2}\left(p^{n+1}_{1}-p^{n+1}_{1-1/2}\right)=G_w\left(\frac{1}{\mu_gB_g}\right)^{n+1}_{1-1/2}\left(p^{n+1}_{1}-p^{n+1}_{wf}\right) \\ =\frac{2\pi\beta_0k_{r_1}\Delta z}{\ln\left(r_1/r_w\right)+s}\left(\frac{1}{\mu_gB_g}\right)^{n+1}_{1-1/2}\left(p^{n+1}_{1}-p^{n+1}_{wf}\right) \quad \text{..... (20)}$$

As can be seen from the previously described equation, the wellbore-first reservoir grid transmissibility $T_{1-1/2}$ is a function of both the wellbore-geometric factor $G_w$ and fluid properties that, in turn, are functions of the reservoir pressure and temperature. The wellbore-geometric factor is also a function of the reservoir properties, grid system, and wellbore radius.

A no-flow (closed) boundary is assumed for the outer reservoir boundary, $T^{n+1}_{N_{res}+1/2}=0$.

## Wellbore

**Mass-Balance Equation.** The wellbore mass-balance equation (Eq. 7) can be discretized in the upwind residual form as

$$R^{n+1}_{mW,\,k}=\frac{A_k\Delta L_k}{\Delta t^{n+1}}\left(\rho^{n+1}_{k}-\rho^{n}_{k}\right) -\left(\rho^{n+1}_{k+1}V^{n+1}_{k+1}A_{k+1}-\rho^{n+1}_{k}V^{n+1}_{k}A_k\right)-m^{n+1}_{k}=0 \quad \text{..... (21)}$$

**Momentum-Balance Equation.** The pressure-drop equation (Eq. 9) can be written in the residual form as

$$R^{n+1}_{momW,\,k}=p^{n+1}_{k}-p^{n+1}_{k-1} -\frac{1}{\beta_1}\left(\Delta p^{n+1}_{h,k}+\Delta p^{n+1}_{f,k}+\Delta p^{n+1}_{a,k}+\Delta p^{n+1}_{u,k}+\Delta p^{n+1}_{perf,k}\right)=0 \quad \text{..... (22)}$$

where

$$\Delta p^{n+1}_{h,k}=\rho^{n+1}_{k}g\cos\left(\theta_k\right)\Delta L_k \quad \text{..... (23)}$$

$$\Delta p^{n+1}_{f,k}=\frac{f^{n+1}_{k}\rho^{n+1}_{k}V^{n+1}_{k}\left|V^{n+1}_{k}\right|}{2d_k}\Delta L_k \quad \text{..... (24)}$$

$$\Delta p^{n+1}_{a,k}=\rho^{n+1}_{k}V^{n+1}_{k}\left(V^{n+1}_{k}-V^{n+1}_{k+1}\right) \quad \text{..... (25)}$$

$$\Delta p^{n+1}_{u,k}=\rho^{n+1}_{k}\frac{V^{n+1}_{k}-V^{n}_{k}}{\Delta t^{n+1}}\Delta L_k \quad \text{..... (26)}$$

$$\Delta p^{n+1}_{perf,k}=\frac{m^{n+1}_{k}\times V^{n+1}_{k}}{A_k} \quad , \quad \text{..... (27)}$$

where $k=2, 3, \ldots, N_{\text{seg}}$.

**Well Constraints.** In this paper, because shut-in, opening, or changing a flow rate is desired at the wellhead, the following constraints are applied to the first top gridblock of the wellbore.

**Rate Constraint.** In the residual form, the rate constraint is

$$R^{n+1}_{RctrlW,\,k}=A_k\rho^{n+1}_{k}V^{n+1}_{k}-\rho_{sc}q_{sc}=0 \quad \text{..... ,(28)}$$

where $k=1$. The subscript $k$ can be also any other grid number than one inside the wellbore. For example, if $k=N_{\text{seg}}$, the rate constraint is applied to the bottomhole condition. In Eq. 28, $q_{sc}$ can vary at

different timesteps to model a multirate schedule and it will be set to zero for shut-in wells. With a negative value of $q_{sc}$, an injection well will be modelled. The wellbore-rate control allows us to simulate the process of closing the wellhead valve as slowly as desired by decreasing the wellhead rate at a few timesteps.

**Pressure Constraint.** Once the WHP drops below a certain value (e.g., 200 psia), the wellhead constraint is switched to a constant WHP as

$$R^{n+1}_{PctrlW,k} = p^{n+1}_{k^{seg}} - p_{target} = 0 \,, \quad \text{..... (29)}$$

where $k=1$.

**Energy-Balance Equation.** Neglecting the axial-thermal conductivity in Eq. 10, which is negligible compared with other terms, particularly in a flowing well, the upwind energy-balance equation in the residual form results in

$$R^{n+1}_{eW,k} = (1+C_T)\frac{\Delta L_k}{\Delta t^{n+1}} A_k \left\{ \left[ \rho\left(u + \frac{V^2}{2g_c J_c}\right) \right]^{n+1}_k - \left[ \rho\left(u + \frac{V^2}{2g_c J_c}\right) \right]^{n}_k \right\}$$
$$- \left\{ \left[ \rho VA\left(h + \frac{V^2}{2g_c J_c}\right) \right]^{n+1}_{k+1} - \left[ \rho VA\left(h + \frac{V^2}{2g_c J_c}\right) \right]^{n+1}_k \right\}$$
$$- A_k \Delta L_k \left[ \frac{g}{g_c J_c} \rho V \cos(\theta) \right]^{n+1}_k + Q^{n+1}_{loss_k} \Delta L_k - m^{n+1}_{h_k} = 0$$
$$\text{..... (30)}$$

## Cement and Tubular Materials and Formation

The tubing outside, casing inside, and wellbore temperatures represented by Eqs. 12 through 14, respectively, can be discretized in the residual form as

$$R^{n+1}_{to_k} = T^{n+1}_{k^{seg}} - \left[\ln(r_{to}/r_{ti})/k_t\right] r_{to} U^{n+1}_{to_k} \left( T^{n+1}_{k^{seg}} - T^{n+1}_{e_{wb,k}} \right) - T^{n+1}_{to_k} = 0$$
$$\text{..... (31)}$$

$$R^{n+1}_{ci_k} = T^{n+1}_{e_{wb,k}} + \left[\ln(r_{wb}/r_{co})/k_{cem} + \ln(r_{co}/r_{ci})/k_c\right]$$
$$\times r_{to} U^{n+1}_{to_k} \left( T^{n+1}_{k^{seg}} - T^{n+1}_{e_{wb,k}} \right) - T^{n+1}_{ci_k} = 0 \quad \text{..... (32)}$$

$$R^{n+1}_{wb,k} = Q^{n+1}_{loss_k} - \Psi_{r_{k,1-1/2}} \left( T^{n+1}_{e_{wb,k}} - T^{n+1}_{e_{k,1}} \right) = 2\pi r_{to} U^{n+1}_{to_k} \left( T^{n+1}_{k^{seg}} - T^{n+1}_{e_{wb,k}} \right)$$
$$- \Psi_{r_{k,1-1/2}} \left( T^{n+1}_{e_{wb,k}} - T^{n+1}_{e_{k,1}} \right) = 0$$
$$\text{..... (33)}$$

Multiplying both sides of the heat-conduction PDE (Eq. 16) by a gridblock volume ($V_{b_{k,i}} = 2\pi r_i \Delta r_i \Delta z_k$), and performing some manipulations, it can be discretized as

$$R^{n+1}_{eF_{k,i}} = \left[ \Psi_{r_{k,i+1/2}} \left( T^{n+1}_{e_{k,i+1}} - T^{n+1}_{e_{k,i}} \right) + \Psi_{r_{k,i-1/2}} \left( T^{n+1}_{e_{k,i-1}} - T^{n+1}_{e_{k,i}} \right) \right]$$
$$+ \left[ \Psi_{z_{k+1/2,i}} \left( T^{n+1}_{e_{k+1,i}} - T^{n+1}_{e_{k,i}} \right) + \Psi_{z_{k-1/2,i}} \left( T^{n+1}_{e_{k-1,i}} - T^{n+1}_{e_{k,i}} \right) \right] \,, \quad \text{..... (34)}$$
$$+ Q^{n+1}_{loss_k} \Delta z_k - \left( V_b \rho_e C_{pe} \right)_{k,i} \frac{T^{n+1}_{e_{k,i}} - T^{n}_{e_{k,i}}}{\Delta t^{n+1}} = 0$$

where the thermal geometric factors are given by

$$\Psi_{r_{k,i\pm1/2}} = \left( \frac{2\pi r \Delta z k_{er}}{\Delta r} \right)_{k,i\pm1/2} = \left( \frac{A_r k_{er}}{\Delta r} \right)_{k,i\pm1/2} \quad \text{..... (35)}$$

$$\Psi_{z_{k\pm1/2,i}} = \left( \frac{2\pi r \Delta r k_{ez}}{\Delta z} \right)_{k\pm1/2,i} = \left( \frac{A_z k_{ez}}{\Delta z} \right)_{k\pm1/2,i} \quad \text{..... (36)}$$

and can be calculated from Appendix B.

The heat conduction PDE has four BCs (see Fig. 1) and one initial condition (IC) given:

**BC 1**: $T_e = T_{\text{surface}}$ at $z=0$, $r \geq r_{wb}$ ..... (37)

**BC 2**: $T_e = T_{\text{reservoir}}$ at $z=L$, $r \geq r_{wb}$ ..... (38)

**BC 3**: $\frac{\partial T_e}{\partial r} = 0$ or $\Psi_{rk,\,Ne+1/2} = 0$ at $0 \leq z \leq L$, $r \to \infty$ ..... (39)

**BC 4**: $Q^{n+1}_{loss_k} = -2\pi r_{wb} k_{er} \left. \frac{\partial T_e}{\partial r} \right|^{n+1}_{r=r_{wb}} = \Psi_{r_{k,\,1-1/2}} \left( T^{n+1}_{e_{wb,k}} - T^{n+1}_{e_{k,\,1}} \right)$ at,
$0 \leq z \leq L$, $r = r_{wb}$ ..... (40)

**IC**: $T^l_{ei} = T^{top\ of\ layer\ l}_{ei} + g^l_T z^l \cos(\theta^l)$, ..... (41)

where $l$ represents the layer number and $g^l_T$ is the geothermal gradient for Layer $l$.

In BC 4, the thermal geometric factor at wellbore radius, $\Psi_{rk,1\text{-}1/2}$, is given by

$$\Psi_{r_{k,1-1/2}} = \frac{2\pi k_{er_{k,1}}}{\ln(r_{k,1}/r_{k,1-1/2}) + TSkin_{k,1-1/2}} \quad \text{..... (42)}$$

In Eq. 42, the first subscript $k$ is the index that indicates the formation layer number and the second subscript shows the position of the formation parameter in the radial direction (i.e., 1 means the radius of the first formation gridblock and 1-1/2 means the wellbore radius, $r_{wb}$). The dependence of the thermal geometric factor on the formation thermal conductivity and thermal skin, as shown in Eq. 15, is now clear from Eq. 42. Eq. 42 also indicates that the thermal geometric factor depends on the gridding system and wellbore radius.

Note that the number of gridblocks in the radial direction and the outer radius of the reservoir and formation can be different. For example, the outer radius of the formation is somewhere at a point beyond which the initial geothermal temperature is never distorted. A radius of 50 ft is typically good for this purpose; however, for extra confidence we choose 500 ft.

After writing all discretized governing equations in the residual form, they were linearized by the classical Newton-Raphson's method, as applied to the linearized equations $\bar{\bar{J}}\vec{\delta}(\vec{x}) = -\vec{R}$, where $\bar{\bar{J}}$ is the Jacobian matrix, $\vec{\delta}(\vec{x})$ is the correction vector, $\vec{x}$ is the unknown vector, and $\vec{R}$ is the residual of equations. Note that because a fully implicit scheme is used, the derivatives of all equations (e.g., the governing equations in the residual form, and gas properties such as compressibility, viscosity, enthalpy, internal energy, formation volume factor, $z$-factor, overall heat-transfer coefficient, and friction factor) must be obtained with respect to such variables as temperature, pressure, and velocity. Because the derivation and statement of these derivatives need huge space, only the final form of the derivatives for the friction factor is reported as an example in Appendix A. A new solution vector is obtained by

$$\vec{x}^{\,v+1}_{n+1} = \vec{x}^{\,v}_{n+1} + \vec{\delta}^{\,v+1}_{n+1}(\vec{x}) \,, \quad \text{..... (43)}$$

where the superscript $\boldsymbol{v}$ is the iteration index. The iteration process is continued until appropriate convergence is achieved. A schematic of the Jacobian matrix is shown in **Fig 2.** The first subscript in the expression of $\boldsymbol{J}$ is the medium for which the residual equations are written and can be the reservoir ($R$), wellbore ($W$), or formation ($F$). The second subscript shows the medium variables with respect to which the derivatives are taken. The derivatives for the well control residual equation are written immediately after the corresponding values for the reservoir part. Converting the non-

| | | |
|---|---|---|
| $J_{RR}$ | $J_{RW}$ | $J_{RF}$ |
| | **Well Control** | |
| $J_{WR}$ | $J_{WW}$ | $J_{WF}$ |
| $J_{FR}$ | $J_{FW}$ | $J_{FF}$ |

**Fig. 2—Schematic representation of the Jacobian matrix.**

isothermal simulator to the isothermal coupled wellbore/reservoir model is quite simple. For this purpose, the last column and row in the Jacobian matrix (Fig. 2), which are for the tubular and cement materials and the formation, will be discarded. In this case, we will not have any derivatives in the Jacobian matrix with respect to temperature and there is no energy equation because the temperature is constant and fixed.

## Results and Discussion

The reservoir part of the simulator, decoupled from other parts (wellbore and formation), is validated with the output results of the IMEX module of Computer Modelling Group (CMG) software (IMEX Advanced Oil/Gas Reservoir Simulator 2009) and the numerical model of F.A.S.T. WellTest software (F.A.S.T. WellTest 2009b) with the same input data for all three simulators. An excellent agreement is seen for the BHP vs. time for all simulators.

To validate the developed simulator as a whole (the coupled reservoir, wellbore, and formation simulator), a multirate test has been performed, with a series of two drawdown and two buildup sequences with the same duration but different flow rates at each drawdown test. In this test, the buildup is allowed to reach semistabilization (i.e., near the initial reservoir pressure). This type of test is quite often performed for gas wells and is called the isochronal test. The input data for the validation are tabulated in **Table 1,** which is a typical set of data for gas reservoirs in the US Gulf Coast (Fan et al. 2000). The results are compared either with the numerical isothermal model that has been developed in this paper or with the analytical models implemented in the F.A.S.T. WellTest software ((F.A.S.T. WellTest 2009b).

**Fig. 3** shows the BHP for drawdowns and buildups and the corresponding wellhead volumetric gas-flow rates as time elapses. The gas-flow rates for the first and second drawdowns are 5 and 8 MMscf/D, respectively. The pressure decreases from an initial pressure of 9,000 psia to 6,134 psia (31.84% drawdown) at the end of the first drawdown and subsequently builds to 8,838.5 psia. Then, pressure drops to 4,287 psia (52.37% drawdown) for the second drawdown and reaches 8,671 psia for the second buildup. As illustrated in Fig. 3, the transient BHP for the developed numerical nonisothermal model and the analytical models inside the well-testing software have a good agreement with each other. Maximum absolute relative errors of 5.3, 2.9, 8.9, and 4.3% in the BHP estimation with the numerical nonisothermal model compared with the analytical models were observed for the first drawdown and buildup and the second drawdown and buildup tests, respectively. These differences are the result of several factors, including some assumptions in the analytical models of the well-testing software. These assumptions are removed in the course of developing our simulator. In addition, thermal effects and the effect of coupling wellbore and formation to the reservoir are considered in our model.

**Figs. 4 and 5** illustrate the pseudopressure drop per rate and derivative plots and the pseudopressure rise and derivative plots vs. pseudotime for the second drawdown and buildup, respectively, for both the developed nonisothermal model and analytical models in the well-testing software. The corresponding semilog plots (traditionally called the Horner semilog plot for the buildup period) are shown in **Figs. 6 and 7.** The terms shown in the *x*- and *y*-axis of Figs. 4 through 7 are common expressions in well testing that can be found in most books that explain a transient pressure analysis or can be found in the user's guide of the F.A.S.T. WellTest software (F.A.S.T. WellTest User's Guide 2009a). As can be seen from Figs. 4 through 7, the early- and late-time periods are quite well matched together; however, large discrepancies can be observed near the middle of the graphs. Furthermore, the discrepancies are more pronounced for the drawdown (Figs. 4 and 6) periods than for the buildup periods (Fig. 5 and 7). For brevity, we have not shown similar plots for the developed isothermal model because these plots are quite similar to the plots for the analytical models (except some small areas in the middle parts because of a variable wellbore-storage coefficient), which also confirms the validation of our models.

**Fig. 8** shows the gas compressibility vs. time at the average wellbore pressure and temperature for both isothermal and nonisothermal models. The difference comes from neglecting temperature-variation effects in the isothermal model (i.e., gas is produced at a fixed reservoir temperature). As expected during the drawdown, the gas compressibility increases as the average wellbore pressure decreases, while in the buildup period, the gas compressibility decreases as the average wellbore pressure increases.

The changing wellbore gas compressibility vs. time in Fig. 8 and the discrepancies in Figs. 4 through 7 all suggest the presence of a variable wellbore-storage coefficient and temperature effects on the behaviour of transient pressure tests. These behaviours will be analyzed thoroughly in Part 2 of this research study (Bahonar et al. 2010).

## Conclusions

The following conclusions can be drawn from this paper:

1. A fully implicit single-phase gas coupled wellbore/reservoir model has been developed by solving the equations of mass, momentum, and energy inside the wellbore and has been validated against analytical models. A feature of this model is the development of a strong heat-loss module for the heat loss from the wellbore to the surrounding medium that increases the overall accuracy of the simulator. The simulator allows computation of transient pressure, temperature, velocity, and fluid properties at any wellbore depth and time, both for shut-in and for flowing wells for imposed surface, reservoir, and well-completion conditions.

2. With the implementation of an EOS into the model, and with its fully implicit nature along with other features, this simulator can be applied for a variety of situations. Examples include running this model for small- to large-timestep sizes; small- to large-wellbore-segment sizes; any gas composition, including sour and corrosive gases; and shallow-to-deep reservoirs (e.g., a hostile environment of HP/HT gas reservoirs). Additionally, allowing gradual opening or closing of the surface valve and capability of running a variety of well tests [e.g., injection, falloff test, and multirate tests (isochronal tests)] are important features of the model.

3. By discarding the last part of the Jacobian matrix that involves the modelling of thermal-resistance components surrounding the wellbore, ignoring all derivatives with respect to temperature, and neglecting the wellbore-energy equation, this nonisothermal model can be converted easily to an equivalent isothermal model.

**TABLE 1—INPUT PARAMETERS FOR VALIDATION OF DEVELOPED NONISOTHERMAL MODEL**

| | |
|---|---|
| Default wellhead constraint (rate or pressure) | constant gas prod. rate |
| Reservoir permeability (md) | 1 |
| Reservoir porosity (fraction) | 0.10 |
| Connate water saturation (fraction) | 0.20 |
| Water compressibility ($psia^{-1}$) | 1.0 E−06 |
| Gas-production rate (MMscf/D) | 5.0 |
| Gas-specific gravity (80% methane and 20% ethane) | 0.651 |
| Gas-critical pressure (psia) | 675.43 |
| Gas-critical temperature (°F) | 384.41 |
| Gas density at standard conditions (lbm/scf) | 0.049845 |
| Geothermal gradient (°F/ft) | 0.0165 |
| Number of reservoir grids | 20 |
| Net pay thickness (ft) | 30 |
| Reservoir area (acre) | 100 |
| Reservoir pressure gradient (psi/ft) | 0.6 |
| Rock compressibility ($psia^{-1}$) | 1.0 E−06 |
| Skin factor | 0 |
| Total depth of the well (ft) | 15,000 |
| Wellhead minimum pressure for switching well constraint (psia) | 200 |
| Wellbore radius (ft) | 0.667 |
| Surface temperature (°F) | 70 |
| Standard condition for pressure (psia) | 14.696 |
| Standard condition for temperature (°F) | 60 |
| Reference pressure for porosity (psia) | 14.7 |
| Wellbore segment length (ft) | 200 |
| Wellbore segment roughness (ft) | 0.000018 |
| Wellbore segment inclination (degree) | 0 |
| Annulus pressure at wellhead (psia) | 14.7 |
| Number of formation (earth) grids in radial direction | 5 |
| Inside radius of tubing (ft) | 0.106167 |
| Outside radius of tubing (ft) | 0.145833 |
| Inside radius of casing (ft) | 0.375000 |
| Outside radius of casing (ft) | 0.447917 |
| Formation (earth) external radius (ft) | 500 |
| Emissivity of casing inside surface (dimensionless) | 0.9 |
| Emissivity of tubing outside surface (dimensionless) | 0.9 |
| Thermal conductivity of tubing [Btu/(sec ft °F)] | 0.006944 |
| Thermal conductivity of casing [Btu/(sec ft °F)] | 0.006944 |
| Thermal conductivity of cementing [Btu/(sec ft °F)] | 0.000320 |
| Thermal conductivity of formation in radial direction [Btu/(sec ft °F)] | 0.000556 |
| Thermal conductivity of formation in axial direction [Btu/(sec ft °F)] | 0.000556 |
| Formation density ($lbm/ft^3$) | 187.2 |
| Formation heat capacity [Btu/(lbm °F)] | 0.186779 |
| Formation thermal diffusivity ($ft^2/sec$) | 1.590160 E−05 |
| Thermal resistance skin factor | 0 |
| Thermal storage parameter | 0 |
| Maximum timestep (sec) | 100,000 |
| Minimum timestep (sec) | 1 |
| Producing time duration (sec) | 200,000 |
| Shut-in time duration (sec) | 200,000 |
| Timestep at the start of production or shut-in (sec) | 1 |
| Tolerance | 1.0 E−06 |

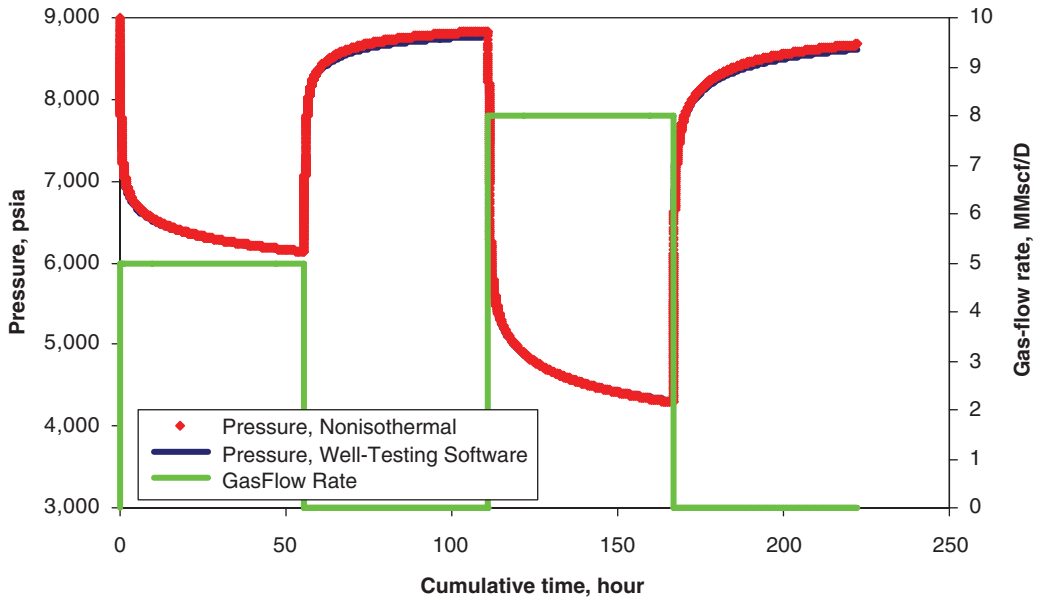


**Fig. 3—BHP and wellhead gas-flow rate vs. time.**

## Nomenclature

$A$ = tubing inside area, ft$^2$
$A_r$ = $2\pi r\Delta z$, area (ft$^2$)
$A_z$ = $2\pi r\Delta r$, area (ft$^2$)
$B_g$ = gas formation volume factor, bbl/scf
$c_R$ = reservoir-rock compressibility, 1/psia
$c'_R$ = combined rock and saturation-weighted water compressibility, 1/psia
$c_w$ = water compressibility, 1/psia
$C_{pe}$ = formation-heat capacity, Btu/(lbm-°F)
$C_T$ = thermal storage parameter, dimensionless
$d$ = internal tubing diameter, ft
$f$ = Moody friction factor, dimensionless
$g$ = acceleration because of gravity, 32.17 ft/sec$^2$
$g_c$ = gravitational conversion constant, 32.17 (ft-lbm)/(lbf-sec$^2$)
$g_T$ = geothermal gradient, °F/ft
$G$ = geometric factor, (bbl-cp)/(psia-sec)
$G_w$ = well geometric factor, (bbl-cp)/(psia-sec)
$h$ = enthalpy, Btu/lbm
$J_c$ = mechanical equivalent of heat, 788 (ft-lbf/Btu)
$\bar{J}$ = Jacobian matrix
$k_c$ = thermal conductivity of casing, Btu/(sec-ft-°F)
$k_{cem}$ = thermal conductivity of cementing, Btu/(sec-ft-°F)
$k_{\mathrm{er}}$ = radial thermal conductivity of formation, Btu/(sec-ft-°F)
$k_{ez}$ = vertical thermal conductivity of formation, Btu/(sec-ft-°F)
$k_f$ = thermal conductivity of fluid inside tubing, Btu/(sec-ft-°F)
$k_r$ = permeability in radial direction, md
$k_t$ = thermal conductivity of tubing, Btu/(sec-ft-°F)
$k_z$ = permeability in vertical direction, md
$L$ = total depth of well, ft
$m$ = mass-transfer rate across the perforation, lbm/sec
$m'$ = mass-transfer rate across the perforation per volume, $\rho q/(\alpha_0 V_b)$, [(lbm-bbl)/(sec-ft$^6$)]
$m_h$ = energy-transfer rate across the perforation, Btu/sec
$N_e$ = number of radial grids in the formation, dimensionless
$N_{\mathrm{res}}$ = number of radial grids in the reservoir, dimensionless
$N_{\mathrm{seg}}$ = number of axial grids in the wellbore, dimensionless
$p$ = pressure, psia
$p_{wf}$ = well-flowing pressure, psia
$q$ = volumetric-flow rate at reservoir condition, ft$^3$/sec
$q_{sc}$ = volumetric-flow rate at the standard condition, scf/sec
$Q_{\mathrm{loss}}$ = heat-loss rate to surroundings per unit wellbore length, Btu/(sec-ft)
$r$ = radius, ft
$r_{ci}$ = inside radius of casing, ft
$r_{co}$ = outside radius of casing, ft
$r_{\mathrm{e}}$ = outer reservoir radius, ft
$r_{ee}$ = outer formation (earth) radius, ft
$r_{ti}$ = inside radius of tubing, ft
$r_{to}$ = outside radius of tubing, ft
$r_{wb}$ = cementing/formation-interface radius (wellbore radius), ft
$R$ = residual of equations
$Re$ = Reynolds number, dimensionless
$s$ = skin factor, dimensionless
$s_{wc}$ = connate-water saturation, dimensionless
$t$ = time, seconds (hours)
$T$ = transmissibility, scf/(psia-sec), except in Eq. 2, which is absolute temperature, °R
$T_{ci}$ = casing inside temperature, °F
$T_e$ = formation temperature, °F
$T^l_{ei}$ = initial formation temperature of Layer $l$, °F
$T_{e_{wb}}$ = cementing/formation-interface temperature (wellbore temperature), °F
$T_f$ = temperature of fluid inside tubing, °F
$T_{\mathrm{reservoir}}$ = reservoir temperature, °F
$T^{\mathrm{seg}}$ = fluid temperature inside tubing, °F
$TSkin$ = thermal skin at $r_{wb}$ caused by thermal resistance, dimensionless
$T_{\mathrm{surface}}$ = surface temperature, °F
$T_{to}$ = tubing outside temperature, °F
$u$ = internal energy, Btu/lbm
$u_r$ = Darcy velocity in radial direction, bbl/(ft$^2$-sec)
$U_{to}$ = overall heat-transfer coefficient, Btu/(sec-ft$^2$-°F)
$V$ = velocity, ft/sec
$V_b$ = gridblock volume, $2\pi r\Delta r\Delta z$, or bulk volume, ft$^3$
$\vec{x}$ = vector of unknowns
$z$ = vertical well depth, ft
$z_g$ = gas $z$-factor, dimensionless
$\alpha_0$ = volume conversion factor, 5.614583 (ft$^3$/bbl)
$\alpha_e$ = formation thermal diffusivity, ft$^2$/sec
$\alpha_{\mathrm{ln}}$ = growth factor in geometrical gridding system, dimensionless

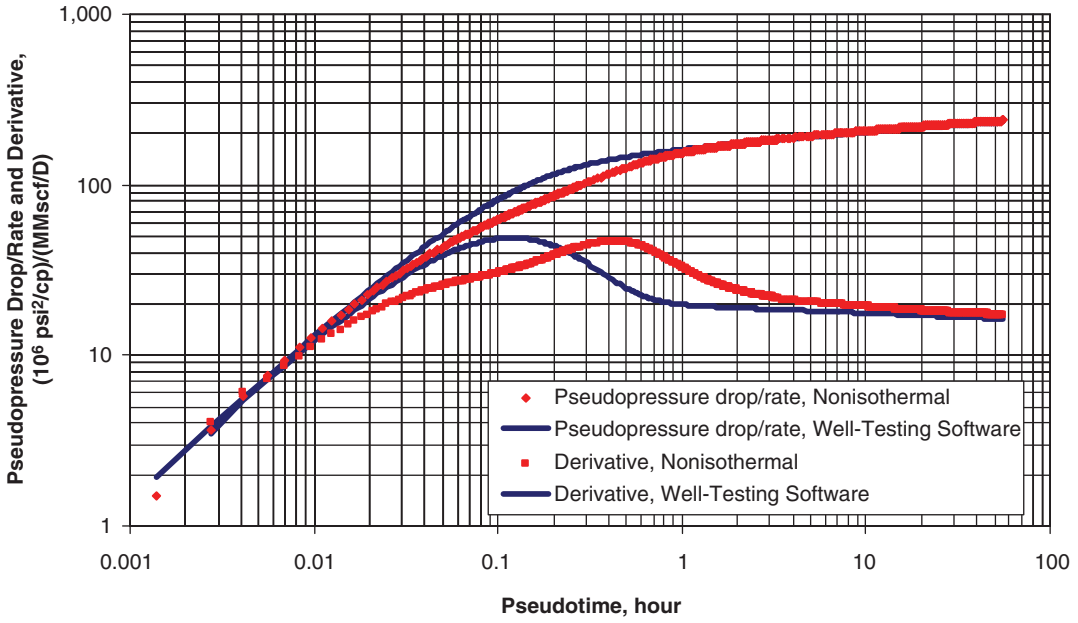


**Fig. 4—Log/log plot of pseudopressure drop per rate and derivative curve vs. pseudotime (drawdown test).**

$\beta_0$ = coefficient of Darcy's law, 0.001127/86400
$\beta_1$ = 144×gc, (in.$^2$/ft$^2$)×(ft-lbm)/(lbf sec$^2$)
$\beta_2$ = 1.0, dimensionless
$\Gamma$ = parameter given in Eqs. 17 and 18, scf/psia
$\delta(\vec{x})$ = correction vector
$\Delta L$ = segment length, ft
$\Delta p_a$ = pressure drop caused by acceleration, lbm/(ft-sec$^2$)
$\Delta p_f$ = pressure drop caused by friction, lbm/(ft-sec$^2$)
$\Delta p_h$ = pressure drop caused by hydrostatic, lbm/(ft-sec$^2$)
$\Delta p_{\text{perf}}$ = pressure drop caused by flow of gas across the perforations, lbm/(ft-sec$^2$)
$\Delta p_u$ = pressure drop caused by unsteadiness, lbm/(ft-sec$^2$)
$\Delta r$ = radial interval, ft
$\Delta t$ = time interval, seconds
$\Delta z$ = axial interval (reservoir formation thickness), ft
$\varepsilon$ = pipe roughness, ft
$\theta$ = local angle between well and the vertical direction, radians
$\mu_g$ = gas viscosity, cp
$\rho$ = density, lbm/ft$^3$
$\rho_e$ = formation density, lbm/ft$^3$
$\rho_{sc}$ = density at standard condition, lbm/scf
$\phi$ = porosity, dimensionless
$\Psi_r$ = thermal geometric factor in radial direction, Btu/(sec-°F)
$\Psi_{rk,\ 1\text{-}1/2}$ = thermal geometric factor at the wellbore, Btu/(sec-ft-°F)
$\Psi_z$ = thermal-geometric factor in axial direction, Btu/(sec-°F)

**Subscripts**

ctrl = control
$i$ = grid discretization index in the $r$-direction
$k$ = grid discretization index in the $z$-direction
ref = reference point
$sc$ = standard condition

**Superscripts**

$l$ = $l^{\text{th}}$ layer in the formation
$n$ = time discretization index
res = reservoir
seg = segment
$v$ = iteration discretization index


## Acknowledgements

The authors would like to thank the Alberta Ingenuity (now part of Alberta Innovates—Technology Futures), Natural Sciences and Engineering Research Council of Canada (NSERC), and the NSERC/Alberta Energy Research Institute (AERI)/iCORE/Foundation CMG Chair Funds for funding this research project. Useful discussions with Silviu Livescu and Mehran Pooladi-Darvish are also gratefully acknowledged. **JCPT**


## References


Abou-Kassem, J.H., Farouq Ali, S.M., and Islam, M.R. 2006. *Petroleum Reservoir Simulation: A Basic Approach*. Houston, Texas: Gulf Publishing Company.

Alves, I.N., Alhanati, F.J.S., and Shoham, O. 1992. A Unified Model for Predicting Flowing Temperature Distribution in Wellbores and Pipelines. *SPE Prod Eng* **7** (6): 363–367. SPE-20632-PA. http://dx.doi.org/10.2118/20632-PA.

Bahonar, M., Azaiez, J., and Chen, Z. 2011. Two Issues in Wellbore Heat Flow Modeling Along With the Prediction of Casing Temperature in the Steam Injection Wells. *J Can Pet Technol* **50** (1): 43–63. SPE-137134-PA. http://dx.doi.org/10.2118/137134-PA.

Bahonar, M., Azaiez, J., and Chen, Z. *In press*. Transient Nonisothermal Fully-Coupled Wellbore/Reservoir Model for Gas-Well Testing, Part 2: Applications. *J Can Pet Technol* (submitted 20 September 2010).

Chen, N.H. 1979. An Explicit Equation for Friction Factor in Pipe. *Ind. Eng. Chem. Fundamen.* **18** (3): 296–297. http://dx.doi.org/10.1021/i160071a019.

Craft, B.C., Hawkins, M., and Terry R.E.1991. *Applied Petroleum Reservoir Engineering*, second edition. Englewood Cliffs, New Jersey: Prentice-Hall.

Ertekin, T., Abou-Kassem, J.H., and King, G.R. 2001. *Basic Applied Reservoir Simulation*. Textbook Series, SPE, Richardson, Texas **7**.

F.A.S.T. WellTest User's Guide, Version 7.1.2.6. 2009a. Calgary, Alberta: Fekete Associates Inc.

F.A.S.T. WellTest, Version 7.1.2.6. 2009b. Calgary, Alberta: Fekete Associates Inc.

Fan, L., Lee, W.J., and Spivey, J.P. 2000. Semi-Analytical Model for Thermal Effect on Gas Well Pressure-Buildup Tests. *SPE Res Eval & Eng* **3** (6): 480–491. SPE-68020-PA. http://dx.doi.org/10.2118/68020-PA.

Farouq Ali, S.M. 1981. A Comprehensive Wellbore Stream/Water Flow Model for Steam Injection and Geothermal Applications. *SPE J.* **21** (5): 527–534. SPE-7966-PA. http://dx.doi.org/10.2118/7966-PA.

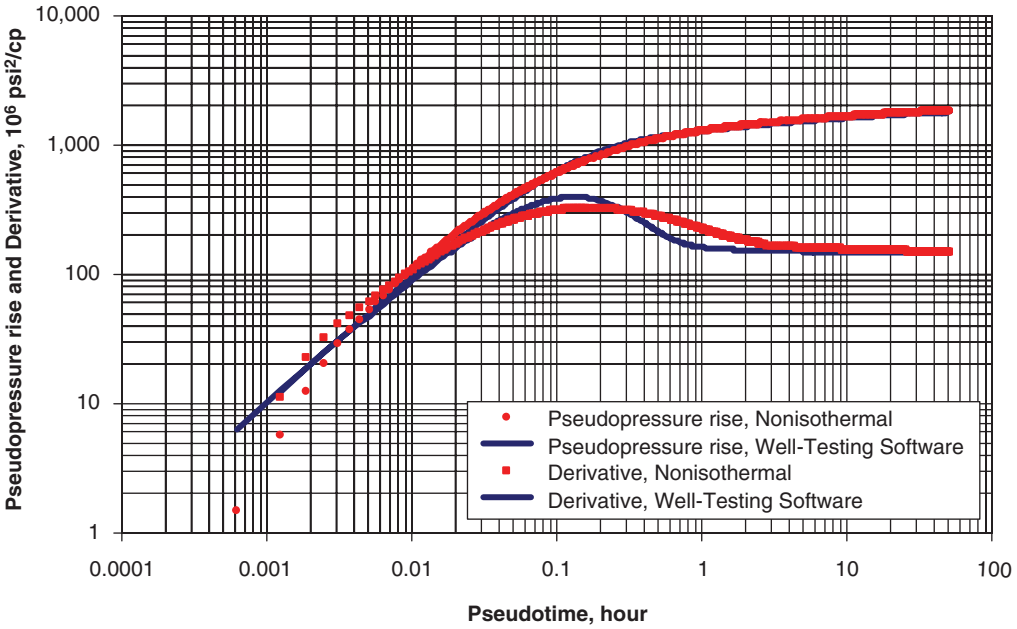


**Fig. 5—Log/log plot of pseudopressure rise and derivative curve vs. pseudotime (buildup test).**


Fontanilla, J.P. and Aziz, K. 1982. Prediction of Bottom-Hole Conditions for Wet Steam Injection Wells. *J Can Pet Technol* **21** (2): 82–88. JCPT Paper No. 82-02-04. http://dx.doi.org/10.2118/82-02-04.

Hasan, A.R. and Kabir, C.S. 1994. Aspects of Wellbore Heat Transfer During Two-Phase Flow. *SPE Prod & Fac* **9** (3): 211–216. SPE-22948-PA. http://dx.doi.org/10.2118/22948-PA.

Hasan, A.R. and Kabir, C.S. 2002. *Fluid Flow and Heat Transfer in Wellbores*. Richardson, Texas: Textbook Series, SPE.

Hasan, A.R. and Kabir, C.S. 2009. Modeling Two-Phase Fluid and Heat Flows in Geothermal Wells. Paper SPE 121351 presented at the SPE Western Regional Meeting, San Jose, California, USA, 24–26 March. http://dx.doi.org/10.2118/121351-MS.

Hasan, A.R., Kabir, C.S., and Lin, D. 2005. Analytic Wellbore-Temperature Model for Transient Gas-Well Testing. *SPE Res Eval & Eng* **8** (1): 240–247. SPE-84288-PA. http://dx.doi.org/10.2118/84288-PA.

Holst, P.H. and Flock, D.L. 1966. Wellbore Behavior During Saturated Steam Injection. *J Can Pet Technol* **5** (4): 184–193. JCPT Paper No. 66-04-05. http://dx.doi.org/10.2118/66-04-05.

IMEX Advanced Oil/Gas Reservoir Simulator, Version 2009.10. 2009. Calgary, Alberta: Computer Modelling Group (CMG).

Izgec, B., Kabir, C.S., Zhu, D., and Hasan, A.R. 2007. Transient Fluid and Heat Flow Modeling in Coupled Wellbore/Reservoir Systems. *SPE Res Eval & Eng* **10** (3): 294–301. SPE-102070-PA. http://dx.doi.org/10.2118/102070-PA.

Kabir, C.S., Hasan, A.R., Jordan, D.L., and Wang, X. 1996. A Wellbore/Reservoir Simulator for Testing Gas Wells in High-Temperature Reservoirs. *SPE Form Eval* **11** (2): 128–134. SPE-28402-PA. http://dx.doi.org/10.2118/28402-PA.

Livescu, S., Durlofsky, L.J., Aziz, K., and Ginestra, J.C. 2010. A fully-coupled thermal multiphase wellbore flow model for use in reservoir simulation. *J. Pet. Sci. Eng.* **71** (3–4): 138–146. http://dx.doi.org/10.1016/j.petrol.2009.11.022.

Miller, C.W. 1980. Wellbore Storage Effect in Geothermal Wells. *SPE J.* **20** (6): 555–566. SPE-8203-PA. http://dx.doi.org/10.2118/8203-PA.

Passut, C.A. and Danner, R.P. 1972. Correlation of Ideal Gas Enthalpy, Heat Capacity, and Entropy. *Ind. Eng. Chem. Process Des. Dev.* **11** (4): 543–546. http://dx.doi.org/10.1021/i260044a016.

Peng, D.-Y. and Robinson, D.B. 1976. A New Two-Constant Equation of State. *Ind. Eng. Chem. Fundamentals* **15** (1): 59–64. http://dx.doi.org/10.1021/i160057a011.

Pourafshary, P., Varavei, A., Sepehrnoori, K., and Podio, L. 2009. A compositional wellbore/reservoir simulator to model multiphase flow and temperature distribution. *J. Pet. Sci. Eng.* **69** (1–2): 40–52. http://dx.doi.org/10.1016/j.petrol.2009.02.012.

Ramey, H.J. Jr. 1962. Wellbore Heat Transmission. *J Pet Technol* **14** (4): 427–435; *Trans.,* AIME, **225**. SPE-96-PA. http://dx.doi.org/10.2118/96-PA.

Sagar, R.K., Doty, D.R., and Schmidt, Z. 1991. Predicting Temperature Profiles in a Flowing Well. *SPE Prod Eng* **6** (6): 441–448. SPE-19702-PA. http://dx.doi.org/10.2118/19702-PA.

Sandler, S.I. 2006. *Chemical, Biochemical, and Engineering Thermodynamics*, fourth edition. Hoboken, New Jersey: John Wiley & Sons.

Satter, A. 1965. Heat Losses During Flow of Steam Down a Wellbore. *J Pet Technol* **17** (7): 845–851. SPE-1071-PA. http://dx.doi.org/10.2118/1071-PA.

Semenova, A., Livescu, S., Durlofsky, L.J., and Aziz, K. 2010. Modeling of Multisegmented Thermal Wells in Reservoir Simulation. Paper SPE 130371 presented at the SPE EUROPEC/EAGE Annual Conference and Exhibition, Barcelona, Spain, 14–17 June. http://dx.doi.org/10.2118/130371-MS.

Shirdel, M. and Sepehrnoori, K. 2009. Development of a Coupled Compositional Wellbore/Reservoir Simulator for Modeling Pressure and Temperature Distribution in Horizontal Wells. Paper SPE 124806 presented at the SPE Annual Technical Conference and Exhibition, New Orleans, 4–7 October. http://dx.doi.org/10.2118/124806-MS.

Stone, T.W., Bennett, J., Law, D.H.-S., and Holmes, J.A. 2002. Thermal Simulation With Multisegment Wells. *SPE Res Eval & Eng* **5** (3): 206–218. SPE-78131-PA. http://dx.doi.org/10.2118/78131-PA.

Stone, T.W., Edmunds, N.R., and Kristoff, B.J. 1989. A Comprehensive Wellbore/Reservoir Simulator. Paper SPE 18419 presented at the SPE Symposium on Reservoir Simulation, Houston, 6–8 February. http://dx.doi.org/10.2118/18419-MS.

Wilhite, G.P. 1967. Over-All Heat Transfer Coefficients in Steam and Hot Water Injection Wells. *J Pet Technol* **19** (5): 607–615. SPE-1449-PA. http://dx.doi.org/10.2118/1449-PA.

WinProp Phase Property Program, Version 2009.10 User Guide. 2009. Calgary, Alberta: Computer Modelling Group (CMG).

Wu, Y.-S. and Pruess, K. 1990. An Analytical Solution for Wellbore Heat Transmission in Layered Formations. *SPE Res Eng* **5** (4): 531–538. SPE-17497-PA. http://dx.doi.org/10.2118/17497-PA.

Yao, S.C. 1985. Fluid Mechanics and Heat Transfer in Steam Injection Wells. MSc thesis, The University of Tulsa, Tulsa, Oklahoma.


**SI Metric Conversion Factors**

acre × 4.046 856 E+03 = $m^2$

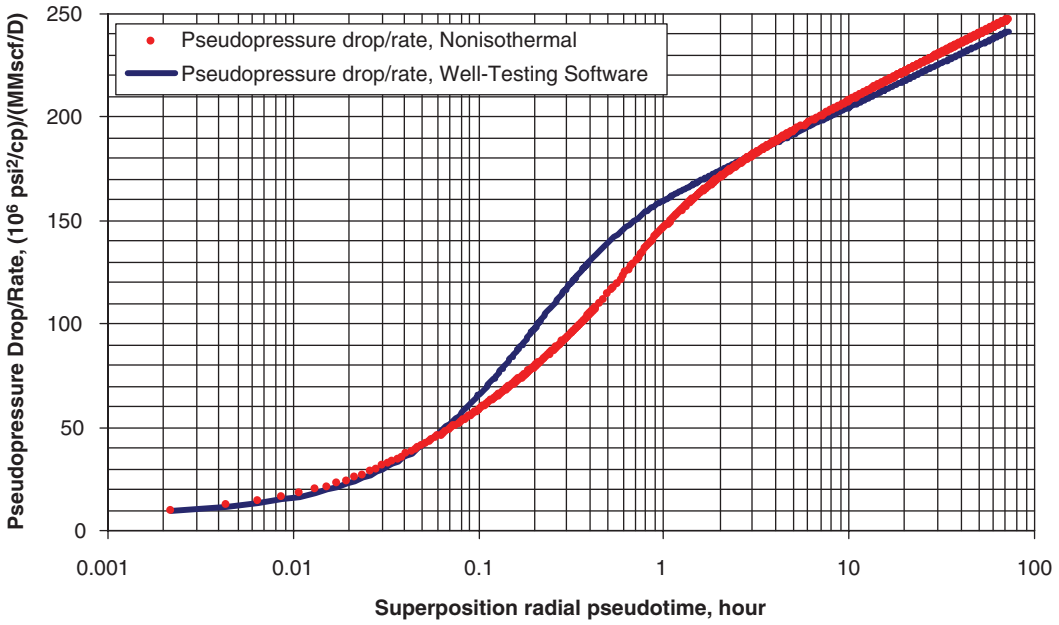


**Fig. 6—Semilog plot of pseudopressure drop per rate vs. superposition radial seudotime (drawdown test).**

| | | | | |
|---|---|---|---|---|
| bbl | × | 1.589 873 | E−01 | = $m^3$ |
| Btu | × | 1.055 056 | E+00 | = kJ |
| Btu/lbm | × | 2.326 | E+03 | = J/kg |
| Btu/(lbm-°F) | × | 4.186 8* | E+03 | = J/(kg·K) |
| Btu/(sec-ft-°F) | × | 6.230 646 | E+03 | = W/(m·K) |
| Btu/(sec-$ft^2$-°F) | × | 2.044 175 | E+04 | = W/($m^2$·K) |
| cp | × | 1.* | E−03 | = Pa·s |
| °F | | (°F−32)/1.8 | | = °C |
| °F/ft | × | 1.822 678 | E+00 | = K/m |
| ft | × | 3.048* | E−01 | = m |
| ft/sec | × | 3.048* | E−01 | = m/s |
| $ft^2$ | × | 9.290 304* | E−02 | = $m^2$ |
| $ft^3$ | × | 2.831 685* | E−02 | = $m^3$ |
| $ft^3$/D | × | 2.831 685* | E−02 | = $m^3$/d |
| lbf | × | 4.44 822 | E+00 | = N |
| lbm | × | 4.535 924 | E−01 | = kg |
| lbm/$ft^3$ | × | 1.601 846 | E+01 | = kg/$m^3$ |
| lbm/sec | × | 4.535 924 | E−01 | = kg/s |
| psia | × | 6.894 757 | E+00 | = kPa |
| $psia^{-1}$ | × | 1.450 377 | E−04 | = $Pa^{-1}$ |
| psia/ft | × | 2.262 059 | E+01 | = kPa/m |
| scf/D | × | 2.863 640 | E−02 | = std $m^3$/d |

*Conversion factor is exact.

## Appendix A

**Friction Factor and Its Derivatives.** Two sets of equations, one set for rough pipes and the other for smooth pipes, are presented.

**Rough Pipes.** Chen's explicit correlation (Chen 1979) for the friction factor in rough pipes is

$$f=\left[a_1\log\left(a_2+\frac{a_3}{\mathrm{Re}}\log(\Lambda)\right)\right]^{a_4}. \quad \text{(A-1)}$$

where $\Lambda=b_1+\left(\frac{b_2}{\mathrm{Re}}\right)^{b_3}$, $b_1=\frac{(\varepsilon/d)^{1.1098}}{2.8257}$, $b_2=7.147$, $b_3=0.8981$, $a_1=2$, $a_2=\frac{\varepsilon/d}{3.7065}$, $a_3=-5.0452$, $a_4=-2$, and the Reynolds number in imperial units is

$$\mathrm{Re}(p,T,V)=1487.873828\frac{\rho(p,T)Vd}{\mu(p,T)} \quad \text{(A-2)}$$

Because our model is solved with a fully implicit scheme, the derivatives of Chen's equation (Chen 1979) with respect to velocity, pressure, and temperature are necessary and are derived and provided here:

$$\frac{\partial f}{\partial V}=-\frac{a_1a_3a_4}{V\,\mathrm{Re}\times\ln(10)}f^{\frac{3}{2}}\left[\log(\Lambda)+\frac{b_3}{\ln(10)\times\Lambda}\right]\left(\frac{b_2}{\mathrm{Re}}\right)^{b_3}\Bigg/\left[a_2+\frac{a_3}{\mathrm{Re}}\log(\Lambda)\right] \quad \text{(A-3)}$$

$$\frac{\partial f}{\partial p}=-V\left(\frac{1}{\mu}\frac{\partial\mu}{\partial p}-\frac{1}{\rho}\frac{\partial\rho}{\partial p}\right)\frac{\partial f}{\partial V} \quad \text{(A-4)}$$

$$\frac{\partial f}{\partial T}=-V\left(\frac{1}{\mu}\frac{\partial\mu}{\partial T}-\frac{1}{\rho}\frac{\partial\rho}{\partial T}\right)\frac{\partial f}{\partial V} \quad \text{(A-5)}$$

**Smooth Pipes.** For smooth pipes and if the Reynolds number is greater than or equal to 2,100 (turbulent flow), Chen's correlation (Chen 1979) for the friction factor is still applicable; otherwise, we use the friction factor for laminar flow, and its derivatives with respect to velocity, pressure, and temperature are

$$f=a\,\mathrm{Re}^b \quad \text{(A-6)}$$

$$\frac{\partial f}{\partial V}=\frac{a\times b\times\mathrm{Re}^b}{V} \quad \text{(A-7)}$$

$$\frac{\partial f}{\partial p}=ab\,\mathrm{Re}^b\left(\frac{1}{\rho}\frac{\partial\rho}{\partial p}-\frac{1}{\mu}\frac{\partial\mu}{\partial p}\right) \quad \text{(A-8)}$$

$$\frac{\partial f}{\partial T}=ab\,\mathrm{Re}^b\left(\frac{1}{\rho}\frac{\partial\rho}{\partial T}-\frac{1}{\mu}\frac{\partial\mu}{\partial T}\right), \quad \text{(A-9)}$$

where $a=64$ and $b=-1.0$.

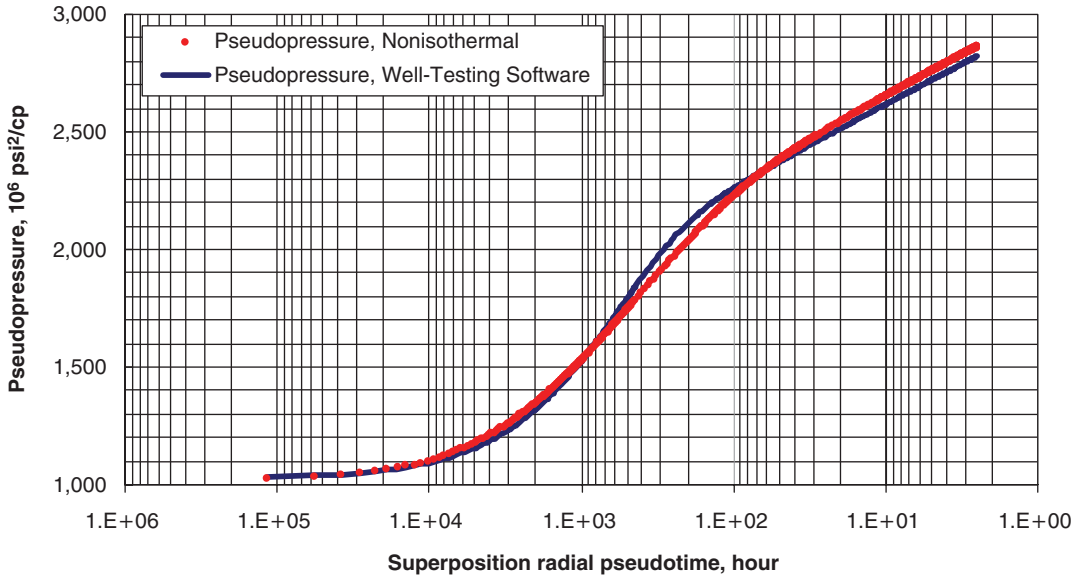


**Fig. 7—Semilog plot of pseudopressure curve vs. superposition radial pseudotime (buildup test).**

## Appendix B

**Grid Scheme.** The grid locations and boundaries, geometric factors for anisotropic formation and irregular grid distributions, and gridblock volumes in a 2D-cylindrical-coordinate system can be calculated by the following equations (Abou-Kassem et al. 2006):

$$\alpha_{\ln}=(r_{ee}/r_{wb})^{(1/N_e)} \quad \text{..... (B-1)}$$

$$r_1=\left[\frac{\alpha_{\ln}\ln(\alpha_{\ln})}{\alpha_{\ln}-1}\right]r_{wb} \quad \text{..... (B-2)}$$

$$r_{i+1}=\alpha_{\ln}r_i=\alpha_{\ln}^i r_1,\ i=1,\ 2,\ \ldots,\ N_e-1 \quad \text{..... (B-3)}$$

$$\Psi_{r_{k,\,i-1/2}}=\frac{2\pi\beta_2}{\ln\left[\alpha_{\ln}\ln(\alpha_{\ln})/(\alpha_{\ln}-1)\right]/(\Delta z_{k,\,i}k_{ez_{k,\,i}})+\ln\left[(\alpha_{\ln}-1)/\ln(\alpha_{\ln})\right]/(\Delta z_{k,\,i-1}k_{ez_{k,\,i-1}})} \quad \text{..... (B-4)}$$

$$\Psi_{r_{k,\,i+1/2}}=\frac{2\pi\beta_2}{\ln\left[(\alpha_{\ln}-1)/\ln(\alpha_{\ln})\right]/(\Delta z_{k,\,i}k_{ez_{k,\,i}})+\ln\left[\alpha_{\ln}\ln(\alpha_{\ln})/(\alpha_{\ln}-1)\right]/(\Delta z_{k,\,i+1}k_{ez_{k,\,i+1}})} \quad \text{..... (B-5)}$$

$$\Psi_{z_{k\pm1/2,\,i}}=\frac{2\beta_2\left(V_{b_{k,\,i}}/\Delta z_{k,\,i}\right)}{\Delta z_{k,\,i}/k_{ez_{k,\,i}}+\Delta z_{k\pm1,i}/k_{ez_{k\pm1,\,i}}} \quad \text{..... (B-6)}$$

$$\begin{cases} V_{b_{k,\,i}}=\pi\dfrac{(\alpha_{\ln}^2-1)^2}{\alpha_{\ln}^2\ln(\alpha_{\ln}^2)}r_i^2\Delta z_k \text{ for } i=1,\ 2,\ \ldots,\ N_e-1,\ k=1,\ 2,\ \ldots,\ N_{seg} \\ V_{b_{k,\,N_e}}=\pi\left\{1-\dfrac{\left[\ln(\alpha_{\ln})/(\alpha_{\ln}-1)\right]^2(\alpha_{\ln}^2-1)}{\alpha_{\ln}^2\ln(\alpha_{\ln}^2)}\right\}r_e^2\Delta z_k \text{ for } i=N_e,\ k=1,\ 2,\ \ldots,\ N_{seg} \end{cases}, \quad \text{..... (B-7)}$$

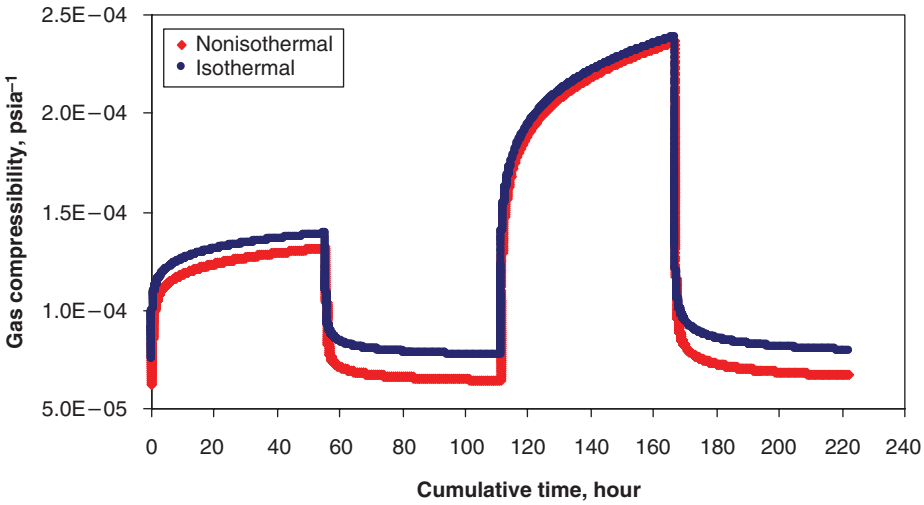


**Fig. 8—Average wellbore gas compressibility vs. time.**

where $\beta_2=1.0$. $\Psi_{rk,\ 1\text{-}1/2}$ and $\Psi_{rk,\ Ne+1/2}$ for the formation (or $G_{rk,\ 1\text{-}1/2}$ and $G_{r_k,\ N_{res}+1/2}$ for the reservoir section) act as the BCs and are calculated by different equations, as given in the body of the paper.

If this grid system is used for the reservoir, $N_e$, $\beta_2$, $k_{er}$, $k_{ez}$, $\Psi_r$, and $r_{ee}$ are replaced by $N_{res}$, $\beta_0$, $k_r$, $k_z$, $G_r$, and $r_e$, respectively. Because a 1D-radial reservoir was considered in this paper, the axial reservoir geometric factor $G_z$ that is the counterpart of the axial formation geometric factor $\Psi_z$ will be meaningless.

## Authors

**Mehdi Bahonar** is a petroleum engineering PhD candidate who joined the Department of Chemical and Petroleum Engineering at the University of Calgary in September 2007 and is currently working at ConocoPhillips Canada as a reservoir engineering intern. He has received several academic awards, scholarships, and bursaries (including the Alberta Ingenuity PhD Graduate Student Scholarship) and authored or coauthored a number of technical and journal papers. Bahonar has conducted research on topics related to steam injection in a fractured heavy-oil carbonate reservoir in Iran, natural convection and thermal radiation in the wellbore annulus, and modelling of transient nonisothermal fluid flow and heat transfer in coupled wellbore/reservoir systems. He holds a BSc degree in petroleum production engineering from the Petroleum University of Technology (PUT) in Iran and dual MSc/MEng degrees in reservoir engineering from the University of Calgary/PUT, both as the first top student. He is a member of SPE and the Association of Professional Engineers, Geologists, and Geophysicists of Alberta.

**Jalel Azaiez** is currently a professor in the Department of Chemical and Petroleum Engineering at the University of Calgary. His expertise is in the field of mathematical modelling and numerical simulation of fluid flows, with a particular focus on complex systems. These include non-Newtonian-fluid flows, rheological modelling of fibre and polymer systems, viscous fingering, and other chemically or thermally driven instabilities in porous media. Azaiez has published more than 40 refereed journal papers, has published more than 20 refereed conference proceedings papers, and has delivered 55 conference talks. He has also presented nine invited talks and seminars worldwide. Azaiez holds a Diplôme d'Ingénieur from the École Centrale de Paris in France and MSc and PhD degrees from Stanford University.

**Zhangxing (John) Chen** is currently a professor at the University of Calgary, is Director of iCentre Simulation and Visualization, and holds the NSERC/AERI/Foundation CMG Senior Research Chair in reservoir simulation and iCORE Industrial Chair in reservoir modelling. He formerly held a Tengfei Chaired and Chang Jiang Chaired Professorship at Xi'an Jiaotong University, Tepin Professorship of Energy and Resources at Peking University, Ziqiang Professorship at Shanghai University, and Gerald J. Ford Research Professorship at Southern Methodist University. Chen holds a BS degree from the University of Jiangxi (China), an MS degree from Xi'an Jiaotong University (China), and a PhD degree from Purdue University, USA.